

Supporting Information

Nature-derived, structure and function integrated ultra-thick carbon electrode for high-performance supercapacitors

Kun Liu,^{ab} Runwei Mo,^a Wujie Dong,^a Wei Zhao,^a Fuqiang Huang^{*ac}

^a State Key Laboratory of High Performance Ceramics and Superfine Microstructure, Shanghai Institute of Ceramics, Chinese Academy of Sciences, Shanghai 200050, P.R. China;

^b Center of Materials Science and Optoelectronics Engineering, University of Chinese Academy of Sciences, 19 Yuquan Road, Beijing 100049, P.R. China;

^c State Key Laboratory of Rare Earth Materials Chemistry and Applications, College of Chemistry and Molecular Engineering, Peking University, Beijing 100871, P.R. China.

* Corresponding authors. E-mail: huangfq@mail.sic.ac.cn

Calculations

Areal capacitance (C_a , F cm⁻²), gravimetric capacitance (C_g , F g⁻¹), and volumetric capacitance (C_v , F cm⁻³) of single electrode and device are calculated based on the GCD curves using the following equations, respectively.

$$C = \frac{I \times t}{\Delta U} \quad (1)$$

$$C_a = \frac{C}{S} \quad (2)$$

$$C_g = \frac{C}{m} \quad (3)$$

$$C_v = \frac{C}{V} \quad (4)$$

where I is the discharge current (A), t is the discharge time (s), ΔU is the operation voltage ($U_{max} - IR_{drop}$). For single electrode, m is the weight of the individual electrode (g), S is the geometric area of electrode (cm²). For the device, m is the weight of the two identical electrodes (g), S is the geometric area of electrode (cm²), and V is the volume of the two identical electrodes (cm³).

Areal energy density (E_a , mWh cm⁻²), and area power density (P_a , mW cm⁻²), of the symmetric device are calculated using the following equations:

$$E_a = \frac{C_a \times \Delta U^2}{2 \times 3.6} \quad (1)$$

$$P_a = \frac{3600 \times E_a}{t} \quad (1)$$

while gravimetric energy density (E_g , Wh kg⁻¹), and volumetric energy density (E_v , mWh cm⁻³) are calculated by replacing C_a with C_g , and C_v , respectively. Gravimetric power density (P_g , W kg⁻¹), and volumetric power density (P_v , mW cm⁻³) are determined by replacing E_a with E_g and E_v , respectively.

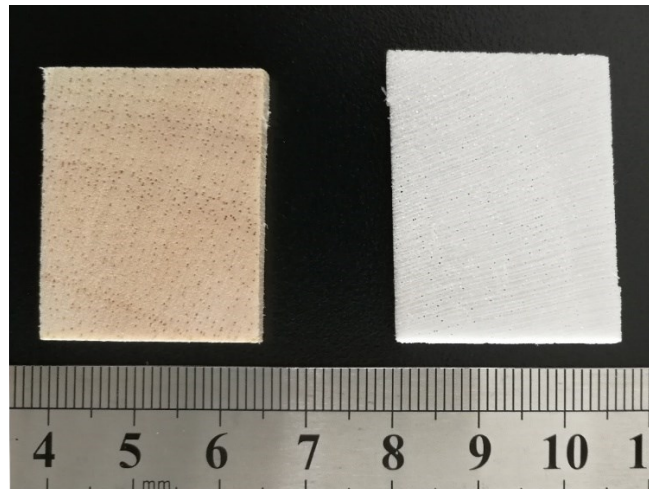


Figure S1. A picture of the natural wood (left) and the as-modified porocellulose (right).

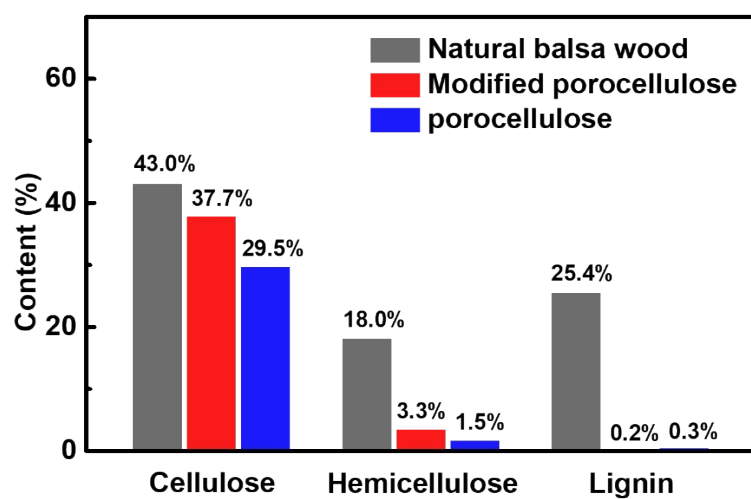
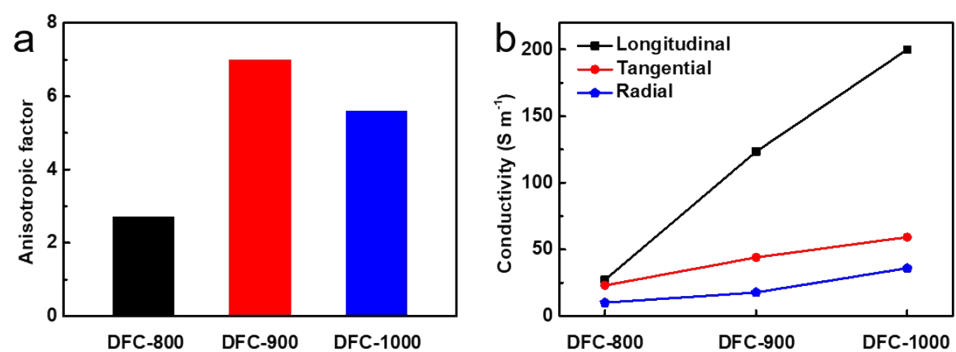


Figure S2. The content of cellulose, hemicellulose, and lignin in the natural balsa wood, modified porocellulose, and porocellulose.



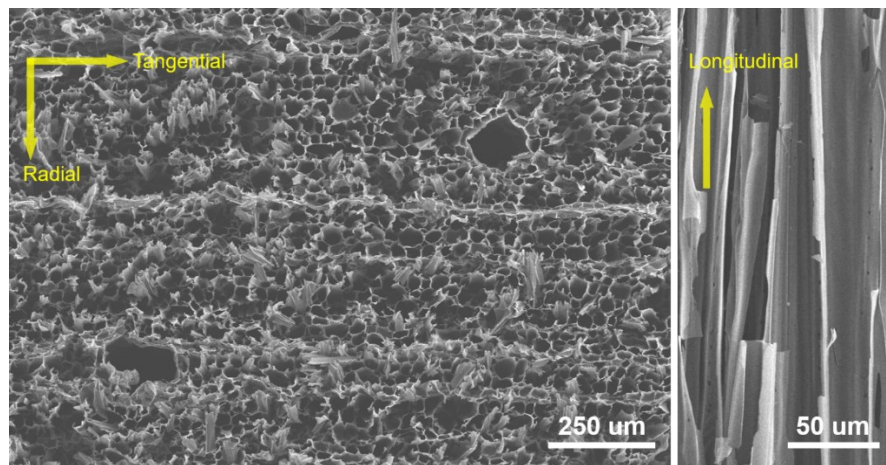


Figure S4. Typical SEM image of DFC-900: (a) top-view image showing the hierarchical grid-like open channels with big channels scattered across uniform small channels, (b) magnified side-view image showing the directional channels along the longitudinal direction after carbonization.

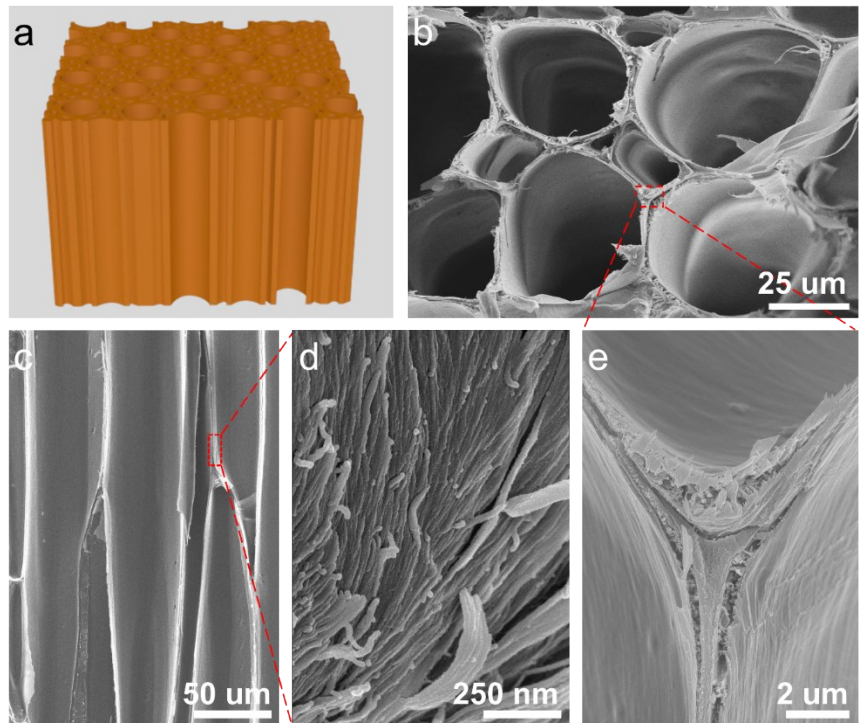


Figure S5. (a) Schematics of the anisotropic multichannel structure of the natural wood. (b) Natural wood showing a hierarchical structural alignment. (c) Side-view SEM image of the aligned channels along the wood growth direction. (d) SEM image of the channel walls composed of aligned nanofibrils. (e) SEM image the multichannel junction glued with the lignin domain.

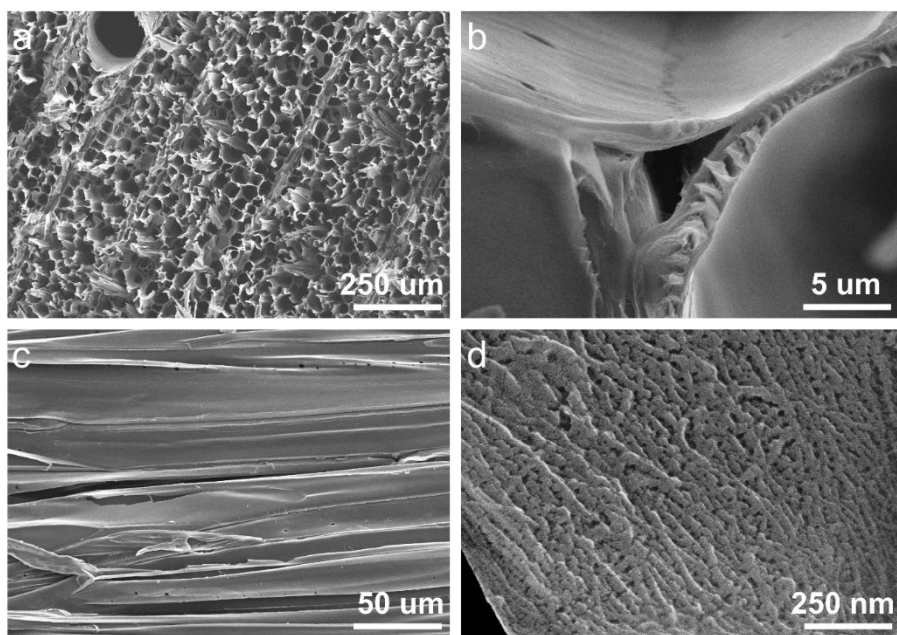


Figure S6. (a) Top-view SEM image of the modified porocellulose. (b) Multichannel ends with a porous junction (c) Side-view SEM image of the aligned channels. (d) Magnified SEM image showing the porous channel walls that composed of isolated aligned nanofibrils in the modified porocellulose.

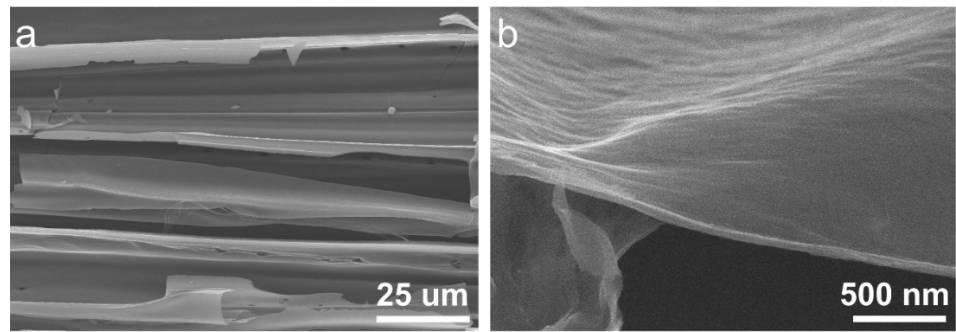


Figure S7. (a) Side-view SEM image of the aligned channels of the DFC-900. (b) Magnified SEM image of the DFC-900 with the corrugated, thin channel walls.

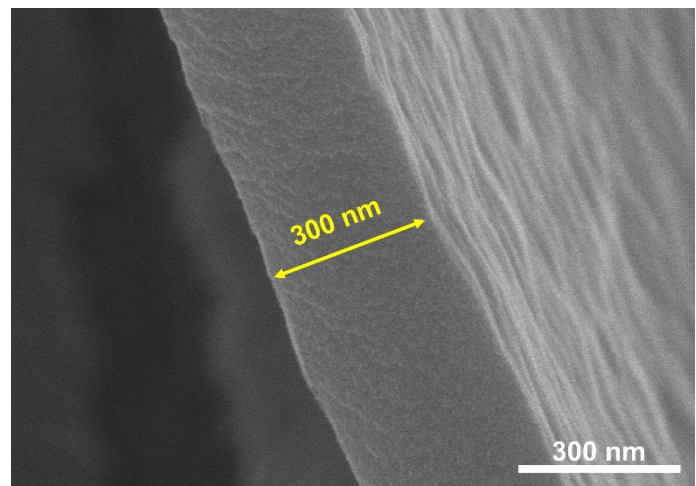


Figure S8. Magnified SEM image of the channel ends

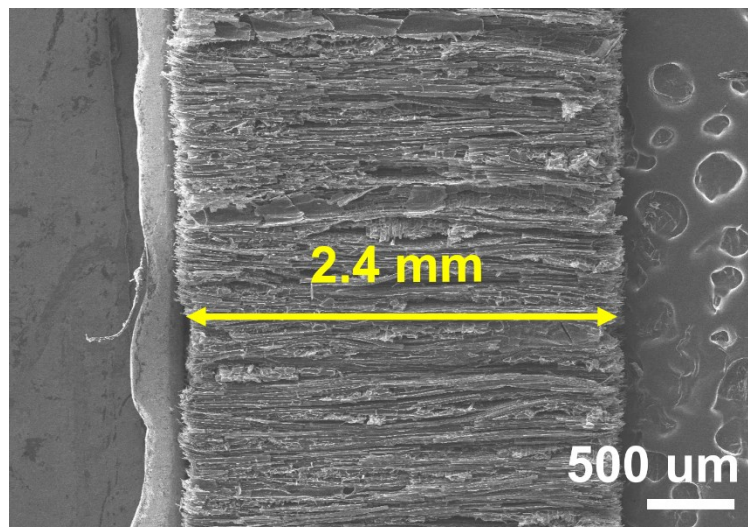


Figure S9. Side-view, showing the thickness of the DFC-900.

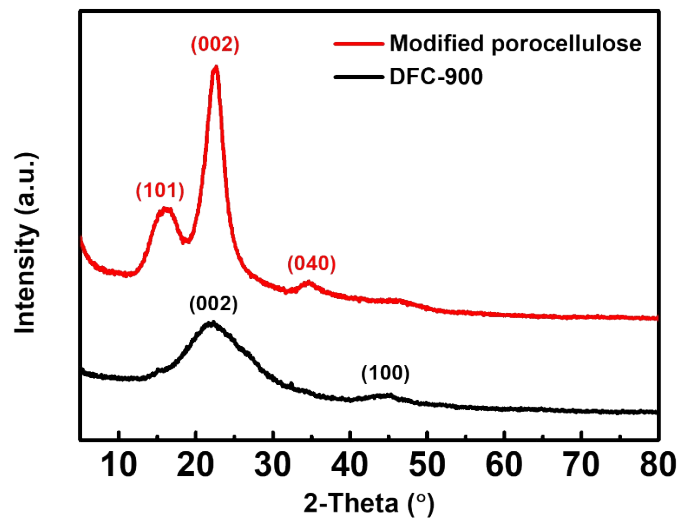


Figure S10. XRD patterns of the modified porocellulose and DFC-900. The XRD patterns were obtained after grounding the modified porocellulose and DFC-900 into powders.

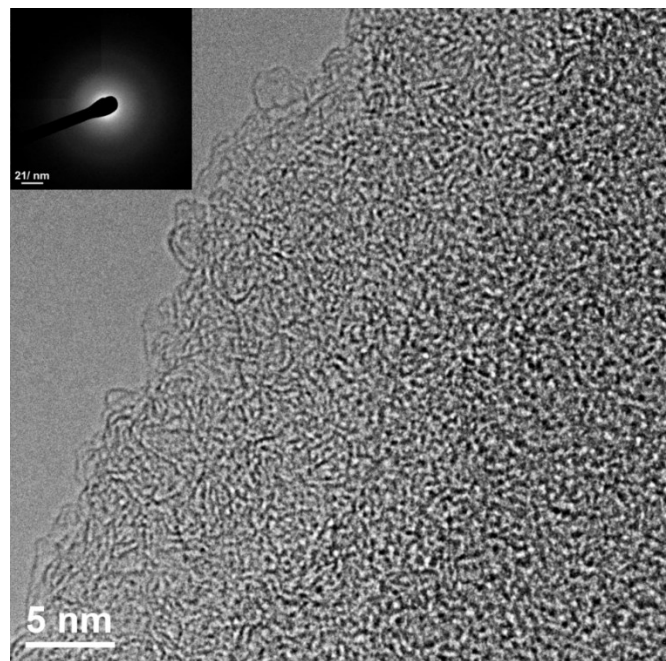


Figure S11. HRTEM image of the DFC-900

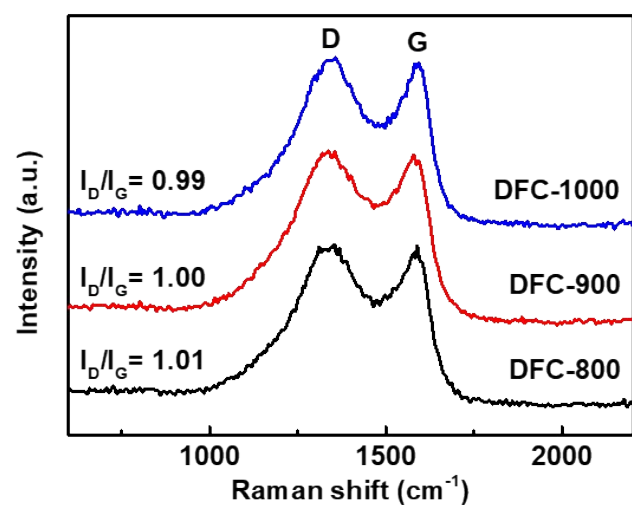


Figure S12. Raman spectra of the DFCs.

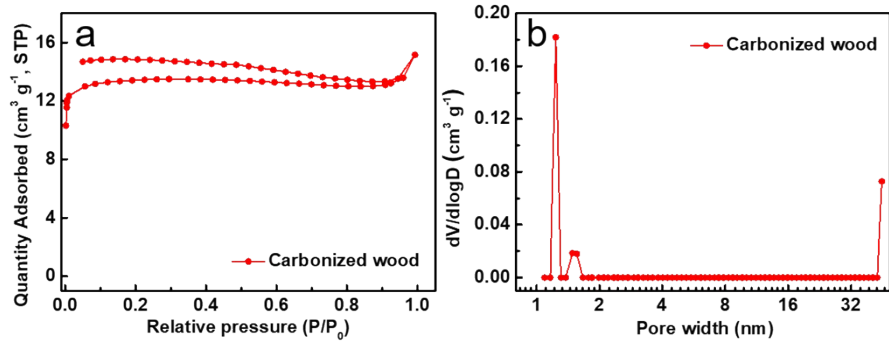


Figure S13. (a) Nitrogen adsorption/desorption isotherms of carbonized wood. (b) The corresponding pore size distribution.

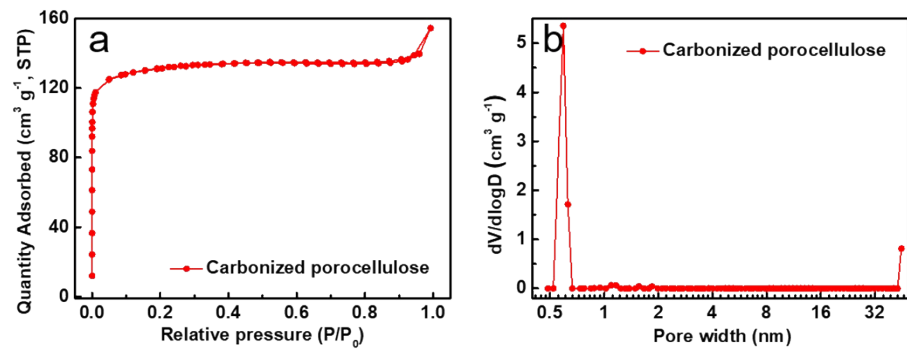


Figure S14. (a) Nitrogen adsorption/desorption isotherms of carbonized porocellulose. (b) The corresponding pore size distribution.

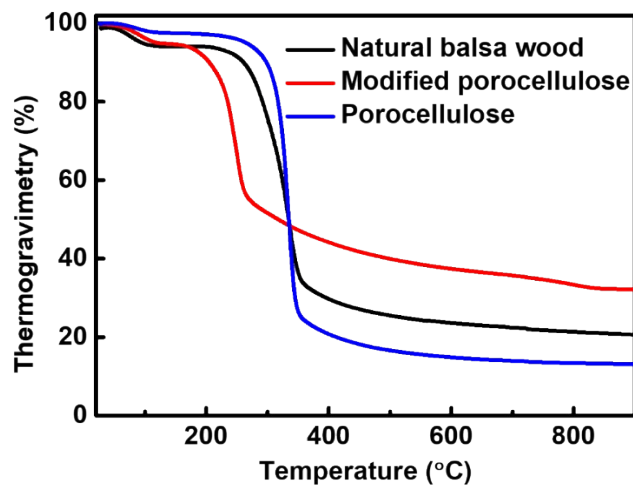


Figure S15. TG curves of natural balsa wood, modified porocellulose, and porocellulose.

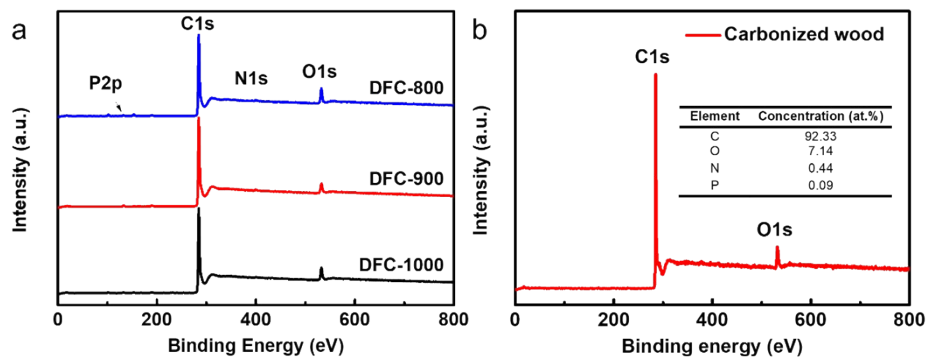


Figure S16. (a) The XPS survey spectra of DFC-800, DFC-900, and DFC-1000. (b) The XPS survey spectrum of carbonized wood. The embedded table shows the corresponding atomic concentrations.

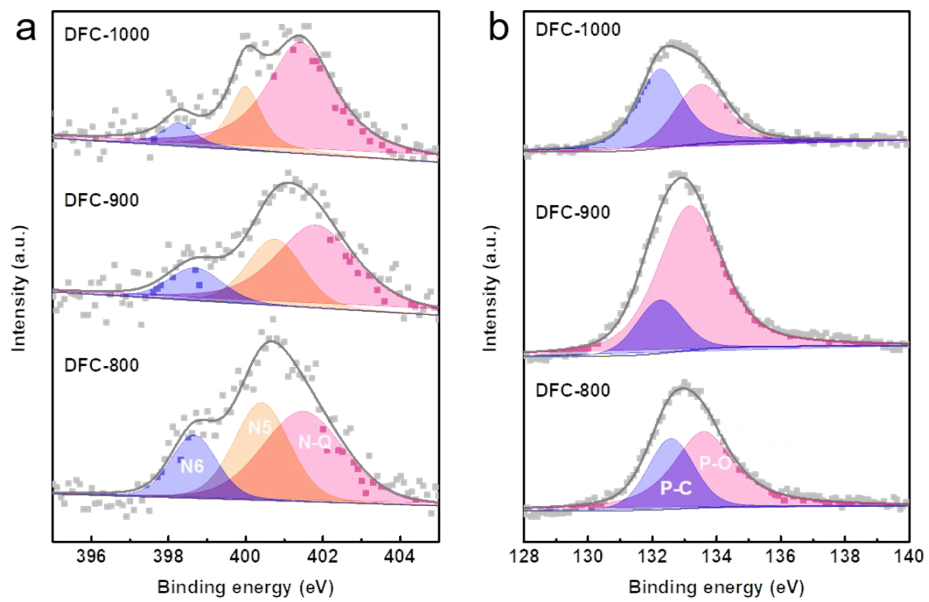


Figure S17. (a) High-resolution N 1s XPS spectra with pyridinic N (N6), pyrrolic N (N5) and graphitic N (N-Q) and (b) P 2p XPS spectra of DFC-800, DFC-900, and DFC-1000, respectively.

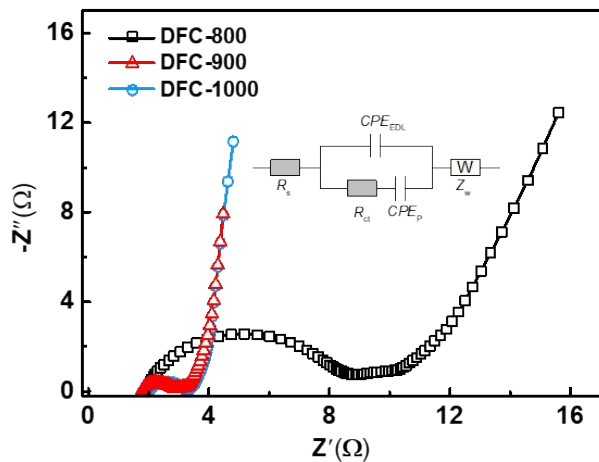


Figure S18. Nyquist plots collected at open circuit potentials with 5mV amplitude and a frequency range from 100000 to 0.01 Hz. The open symbols are experimental data and the solid lines are fitting curves. The Nyquist plots were fitted using the equivalent electric circuit model. R_s : series resistance; R_{ct} : charge transfer resistance; CPE_{EDL} : constant phase element representing the electrical double layer capacitance (EDLC); CPE_p : constant phase element representing the pseudocapacitance; Z_w : Warburg diffusion element.

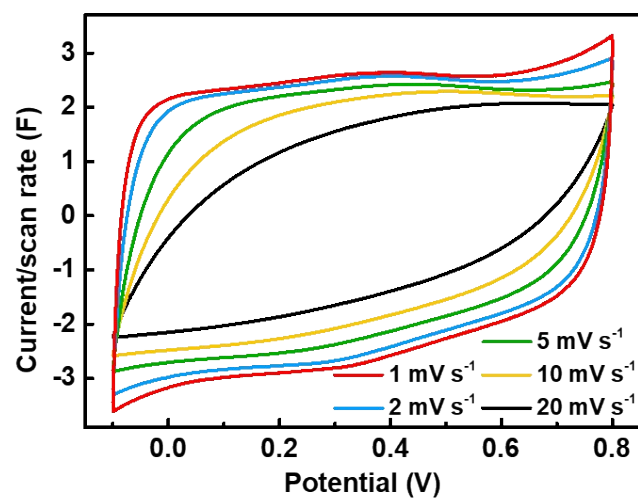


Figure S19. CV curves of DFC-900 at voltage scan rates of 1-20 mV s⁻¹.

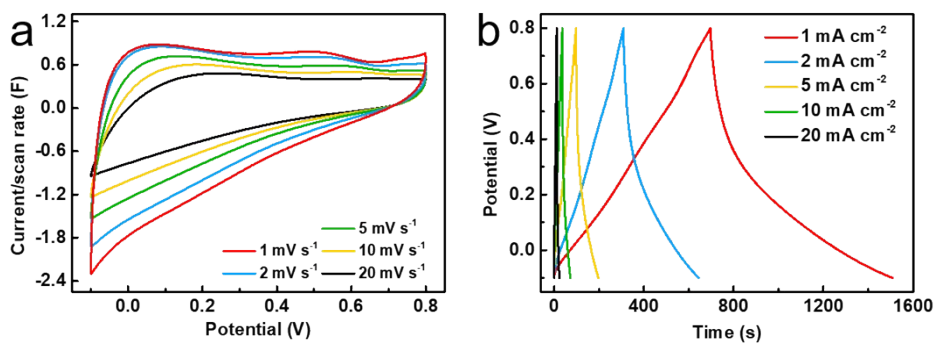


Figure S20. (a) CV curves of carbonized wood at voltage scan rates of 1-20 mV s⁻¹. (b) GCD profiles at current densities of 1-20 mA cm⁻².

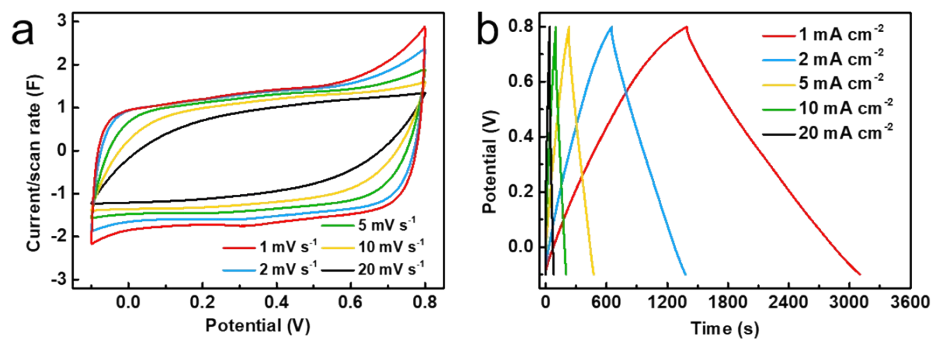


Figure S21. (a) CV curves of carbonized porocellulose at voltage scan rates of $1\text{-}20\text{ mV s}^{-1}$. (b) GCD profiles at current densities of $1\text{-}20\text{ mA cm}^{-2}$.

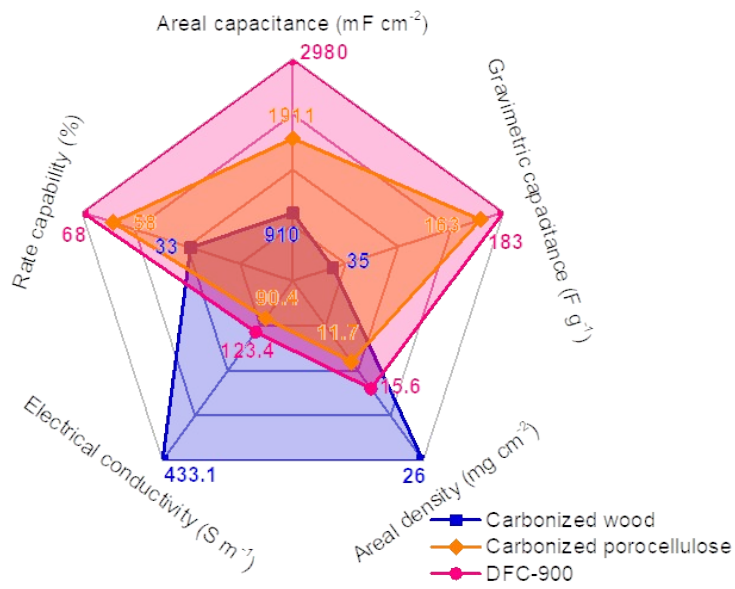


Figure S22. The radar chart compares the five figure-of-merits of carbonized wood (blue), carbonized porocellulose (orange) and DFC-900 (red): areal capacitance normalized to the geometric area, gravimetric capacitance based on the mass of the carbon frameworks, areal density, electrical conductivity along the thick direction, and rate capability (from 1 to 20 mA cm^{-2}). All capacitances are obtained at 1 mA cm^{-2} .

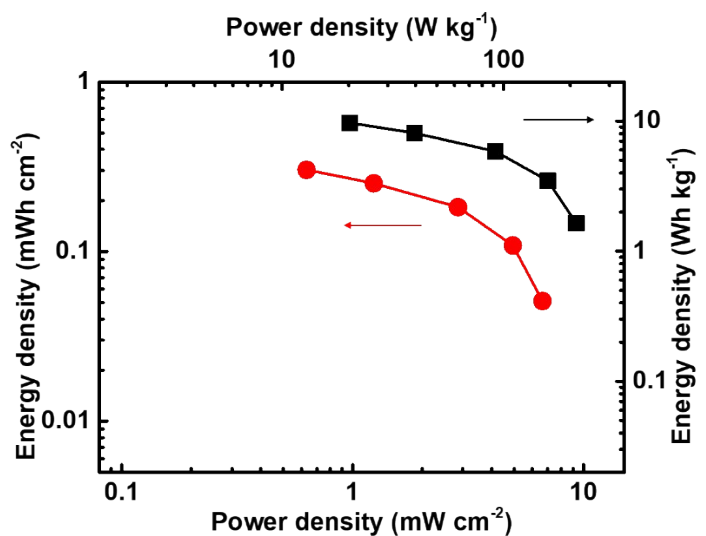


Figure S23. Ragone plot of areal and gravimetric energy density versus power density for the DFC-900 device. The energy and power densities are normalized by the geometric area or total weight of the two electrodes.

Table S1. Areal capacitance comparison of various representative carbon-based electrodes.

Electrodes	Thickness ^a (μm)	Electrolyte	Areal Capacitance	Supporting substrates	Ref.
NFCN2-900	48.1	2M H ₂ SO ₄	612 mF cm ⁻² (1.37 mA cm ⁻²)	Self-supporting	[1]
rGO-2	ca.4500	—	293.4 mF cm ⁻² (2 mA cm ⁻²)	NiP/polymer	[2]
N,P-CNF/GN/BC	320	1M H ₂ SO ₄	2588 mF cm ⁻² (2 mA cm ⁻²)	Bacterial cellulose	[3]
rGO films	250	1M H ₂ SO ₄	915 mF cm ⁻² (1 mA cm ⁻²)	Self-supporting	[4]
3D G	1000	3M LiCl	ca.21 mF cm ⁻² (0.5 mA cm ⁻²)	Self-supporting	[5]
ONCC-60	—	6M KOH	1385 mF cm ⁻² (1 mA cm ⁻²)	Self-supporting	[6]
GNCN film	4.44	6M KOH	147 mF cm ⁻² (5 mV s ⁻¹)	Nickel foam	[7]
B/N-GCM	ca.100	6M KOH	3100 mF cm ⁻² (5 mA cm ⁻²)	Self-supporting	[8]
PCNTAs@CFs	—	6M KOH	20.8 mF cm ⁻² (1 mA cm ⁻²)	Flexible carbon fibers	[9]
Si/TiC/CDC film	5	1M H ₂ SO ₄	205 mF cm ⁻² (1 mV s ⁻¹)	Si/TiC	[10]
EACC-10	—	5M LiCl	756 mF cm ⁻² 6 mA cm ⁻²	Self-supporting	[11]
CW	680	2M KOH	3274 mF cm ⁻² (1 mA cm ⁻²)	Self-supporting	[12]
NCF	4000	5M LiCl	332 mF cm ⁻² (1 mA cm ⁻²)	Self-supporting	[13]
CNC-MWCNT-PPy	ca.10000	0.5 M Na ₂ SO ₄	2100 mF cm ⁻² (2 mV s ⁻¹)	CNC-MWCNT aerogel	[14]
M-NGM	ca.360	1M H ₂ SO ₄	910 mF cm ⁻² (1 A g ⁻¹)	Self-supporting	[15]
RTG	—	3M KCl	820 mF cm ⁻² (5 mA cm ⁻²)	Self-supporting	[16]
AWC	ca.1000	1 M Na ₂ SO ₄	3204 mF cm ⁻² (1 mA cm ⁻²)	Self-supporting	[17]
G-N-Ox	5000	3M KOH	108.88 mF cm ⁻² (0.5 mA cm ⁻²)	Copper foil	[18]
3DG-N-Ox	1000		693 mF cm ⁻² (0.5 Ag ⁻¹)		
GO-GNP-SiO ₂ -2	1000	3M KOH	413.4 mF cm ⁻² (10 A g ⁻¹)	Self-supporting	[19]
CTAs@NCBs-700(T)	ca.333	1M H ₂ SO ₄	366 mF cm ⁻² (1 mA cm ⁻²)	Carbon cloth	[20]
DFC-900	2400	1M H ₂ SO ₄	2980 mF cm ⁻² (1 mA cm ⁻²)	Self-supporting	This work

^aThickness of electrodes are calculated based on the entire electrode including the supporting substrate, if non-self-supporting electrodes are utilized.

Table S2. Areal capacitance and gravimetric capacitance comparison of carbon-based symmetric capacitor devices.

Supercapacitors	Electrode thickness (μm)	Electrolyte	Areal Capacitance	Gravimetric Capacitance	Supporting substrates	Ref.
rGO-2 QSSC	<i>ca.</i> 4500	PVA/KOH	57.75 mF cm^{-2} (1.5 mA cm^{-2})	13.1 F g^{-1} (1.5 A g^{-1})	NiP/polymer	[2]
GP ₁₂ -based ASSC	<i>ca.</i> 96	PVA/H ₂ SO ₄	1104 mF cm^{-2} (4.8 mA cm^{-2})	46 F g^{-1} (0.2 A g^{-1})	Self-supporting	[21]
CNC-MWCNT-PPy SSC	<i>ca.</i> 10000	0.5 M Na ₂ SO ₄	560 mF cm^{-2} (2 mA cm^{-2})	45.6 F g^{-1} (2 mA cm^{-2})	Self-supporting	[14]
C-Web@Ni-Cotton SSC	—	1 M Na ₂ SO ₄	275.8 mF cm^{-2} (1 mA cm^{-2})	—	Nickel-coated cotton fabric	[22]
HAGFF SSC	150	1M H ₂ SO ₄	530 mF cm^{-2} (1 mA cm^{-2})	61 F g^{-1} (0.1 A g^{-1})	Self-supporting	[23]
NFCN2-900 ASSC	48.1	PVA/KOH	240.5 mF cm^{-2} (1.37 mA cm^{-2})	41.1 F g^{-1} 0.25 A g^{-1}	Self-supporting	[1]
rGCN-DC ASSC	1000	PVA/H ₃ PO ₄	1450 mF cm^{-2} (0.5 A g^{-1})	38.1 F g^{-1} (0.5 A g^{-1})	Self-supporting	[24]
GH-f based SC	110	1M H ₂ SO ₄	<i>ca.</i> 1034 mF cm^{-2} (0.1 A g^{-1})	43 F g^{-1} (0.1 A g^{-1})	Self-supporting	[25]
N, P-CNF/GN/BC SSC	320	1M H ₂ SO ₄	898 mF cm^{-2} (2 mA cm^{-2})	—	Bacterial cellulose	[3]
rGO film-based ASSC	250	PVA/H ₂ SO ₄	178 mF cm^{-2} (1 mA cm^{-2})	70.5 F g^{-1} (0.5 A g^{-1})	Carbon paper	[4]
3D GCA QSSC	1000	3M KOH	308.4 mF cm^{-2} (13 mA cm^{-2})	23.7 F g^{-1} (2 A g^{-1})	Self-supporting	[19]
3D porous RGO ASSC	64.7	PVA/H ₃ PO ₄	123 mF cm^{-2}	60.4 F g^{-1}	Self-supporting	[26]
Inked textile ASSC	<i>ca.</i> 330	PVA/LiCl	36 mF cm^{-2} (5 mV s^{-1})	2.93 F g^{-1} (5 mV s^{-1})	Self-supporting	[27]
CDC film MSC	1.4	1M H ₂ SO ₄	24.5 mF cm^{-2} (1 mA cm^{-2})	—	Si wafer	[10]
AG-MSC	4	PVA/H ₂ SO ₄	<i>ca.</i> 89.5 mF cm^{-2} (10 mV s^{-1})	—	SiO ₂ /Si wafer	[28]
PPD-graphene film SSC	<i>ca.</i> 5.5	1M H ₂ SO ₄	355.5 mF cm^{-2} (0.5 A g^{-1})	114.7 F g^{-1} (0.5 A g^{-1})	Self-supporting	[29]
NCF SSC	4000	PVA/LiCl	129 mF cm^{-2} (1 mA cm^{-2})	10.3 F g^{-1} (1 mA cm^{-2})	Self-supporting	[13]
rGO/MWCNT SSC	—	1M H ₂ SO ₄	—	76.25 F g^{-1} (1 A g^{-1})	Stainless-steel gauze	[30]
PG/HQ-PSSs MSC	0.7	PVA/H ₂ SO ₄	9.8 mF cm^{-2} (1 mV s^{-1})	—	PET film	[31]
rGO-MWNTMS SSC	—	6M KOH	148 mF cm^{-2} (0.2 A g^{-1})	24.5 F g^{-1} (0.2 A g^{-1})	Nickel foam	[32]
HPC SSC	<i>ca.</i> 15	6M KOH	—	55 F g^{-1} (5 mV s^{-1})	Self-supporting	[33]
CTAs@NCBs-700(T) SSC	<i>ca.</i> 333	1M H ₂ SO ₄	580 mF cm^{-2} (1 mA cm^{-2})	—	Carbon cloth	[20]
rGOP SSC	3000	1M H ₂ SO ₄	41.6 mF cm^{-2} (8.4 mA cm^{-2})	—	Self-supporting	[34]
Graphene/MWCNT MDHA SSC	2000	6M KOH	639.56 mF cm^{-2} (4 mA cm^{-2})	26.6 F g^{-1} (4 mA cm^{-2})	Self-supporting	[35]
LPG-MSC	6	PVA/LiCl	3.9 mF cm^{-2} (0.3 mA cm^{-2})	—	PET film	[36]

3D-GCA QSSC	1000	LiOH/PVA	308.4 mF cm^{-2} (26 mA cm $^{-2}$)	23.7 F g^{-1} (2 A g $^{-1}$)	Self-supporting	[19]
3DGC-1 SSC	300	1M H ₂ SO ₄	1281 mF cm^{-2} (12 mA cm $^{-2}$)	53 F g^{-1} (0.5 A g $^{-1}$)	Self-supporting	[37]
DFC-900 QSSC	2400	PVA/H ₂ SO ₄	1363 mF cm^{-2} (1 mA cm $^{-2}$)	44 F g^{-1} (1 mA cm $^{-2}$)	Self-supporting	This work

References

- 1 H. Chen, T. Liu, J. Mou, W. Zhang, Z. Jiang, J. Liu, J. Huang and M. Liu, *Nano Energy*, 2019, **63**, 103836.
- 2 J. Xue, L. Gao, X. Hu, K. Cao, W. Zhou, W. Wang and Y. Lu, *Nano-Micro Lett.*, 2019, **11**, 46.
- 3 R. Liu, L. Ma, J. Mei, S. Huang, S. Yang, E. Li and G. Yuan, *Chem. - Eur. J.*, 2017, **23**, 2610-2618.
- 4 L. Zhang, C. Yang, N. Hu, Z. Yang, H. Wei, C. Chen, L. Wei, Z. J. Xu and Y. Zhang, *Nano Energy*, 2016, **26**, 668-676.
- 5 B. Yao, S. Chandrasekaran, J. Zhang, W. Xiao, F. Qian, C. Zhu, E. B. Duoss, C. M. Spadaccini, M. A. Worsley and Y. Li, *Joule*, 2019, **3**, 459-470.
- 6 Y. Zheng, W. Zhao, D. Jia, L. Cui and J. Liu, *Chem. Eng. J.*, 2019, **364**, 70-78.
- 7 L. Jiang, L. Sheng, C. Long and Z. Fan, *Nano Energy*, 2015, **11**, 471-480.
- 8 W. Zhang, S. Wei, Y. Wu, Y.-L. Wang, M. Zhang, D. Roy, H. Wang, J. Yuan and Q. Zhao, *ACS nano*, 2019, **13**, 10261-10271.
- 9 G. Zhang, Y. Song, H. Zhang, J. Xu, H. Duan and J. Liu, *Adv. Funct. Mater.*, 2016, **26**, 3012-3020.
- 10 P. Huang, C. Lethien, S. Pinaud, K. Brousse, R. Laloo, V. Turq, M. Respaud, A. Demortiere, B. Daffos and P.-L. Taberna, *Science*, 2016, **351**, 691-695.
- 11 W. Wang, W. Liu, Y. Zeng, Y. Han, M. Yu, X. Lu and Y. Tong, *Adv. Mater.*, 2015, **27**, 3572-3578.
- 12 Y. Wang, X. Lin, T. Liu, H. Chen, S. Chen, Z. Jiang, J. Liu, J. Huang and M. Liu, *Adv. Funct. Mater.*, 2018, **28**, 1806207.
- 13 K. Xiao, L. X. Ding, G. Liu, H. Chen, S. Wang and H. Wang, *Adv. Mater.*, 2016, **28**, 5997-6002.
- 14 K. Shi, X. Yang, E. D. Cranston and I. Zhitomirsky, *Adv. Funct. Mater.*, 2016, **26**, 6437-6445.
- 15 X. Wang, Y. Ding, F. Chen, H. Lu, N. Zhang and M. Ma, *ACS Appl. Energy Mater.*, 2018, **1**, 5024-5032.
- 16 Y. Song, T.-Y. Liu, G.-L. Xu, D.-Y. Feng, B. Yao, T.-Y. Kou, X.-X. Liu and Y. Li, *J. Mater. Chem. A*, 2016, **4**, 7683-7688.
- 17 C. Chen, Y. Zhang, Y. Li, J. Dai, J. Song, Y. Yao, Y. Gong, I. Kierzewski, J. Xie and L. Hu, *Energy Environ. Sci.*, 2017, **10**, 538-545.
- 18 T. Liu, C. Zhu, T. Kou, M. A. Worsley, F. Qian, C. Condes, E. B. Duoss, C. M. Spadaccini and Y. Li, *ChemNanoMat*, 2016, **2**, 635-641.
- 19 C. Zhu, T. Liu, F. Qian, T. Y.-J. Han, E. B. Duoss, J. D. Kuntz, C. M. Spadaccini, M. A. Worsley and Y. Li, *Nano Lett.*, 2016, **16**, 3448-3456.
- 20 Z. Tang, G. Zhang, H. Zhang, L. Wang, H. Shi, D. Wei and H. Duan, *Energy Storage Mater.*, 2018, **10**, 75-84.
- 21 M. Zhang, X. Yu, H. Ma, W. Du, L. Qu, C. Li and G. Shi, *Energy Environ. Sci.*, 2018, **11**, 559-565.
- 22 Q. Huang, L. Liu, D. Wang, J. Liu, Z. Huang and Z. Zheng, *J. Mater. Chem. A*, 2016, **4**, 6802-6808.
- 23 Z. Li, T. Huang, W. Gao, Z. Xu, D. Chang, C. Zhang and C. Gao, *ACS Nano*, 2017, **11**, 11056-11065.
- 24 B. S. Kim, K. Lee, S. Kang, S. Lee, J. B. Pyo, I. S. Choi, K. Char, J. H. Park, S.-S. Lee and J. Lee, *Nanoscale*, 2017, **9**, 13272-13280.
- 25 M. Sevilla, G. A. Ferrero, T. T. Vu and A. B. Fuertes, *ChemNanoMat*, 2016, **2**, 33-36.

- 26 Y. Shao, M. F. El - Kady, C. W. Lin, G. Zhu, K. L. Marsh, J. Y. Hwang, Q. Zhang, Y. Li, H. Wang and R. B. Kaner, *Adv. Mater.*, 2016, **28**, 6719-6726.
- 27 K. Jo, C.-H. Kim, S. Won, Y. Hwangbo, J.-H. Kim, H.-J. Lee and S.-M. Lee, *J. Mater. Chem. A*, 2016, **4**, 4082-4088.
- 28 Z.-S. Wu, S. Yang, L. Zhang, J. B. Wagner, X. Feng and K. Müllen, *Energy Storage Mater.*, 2015, **1**, 119-126.
- 29 G. Lian, C.-C. Tuan, L. Li, S. Jiao, K.-S. Moon, Q. Wang, D. Cui and C.-P. Wong, *Nano Lett.*, 2017, **17**, 1365-1370.
- 30 Y. Lin, F. Liu, G. Casano, R. Bhavsar, I. A. Kinloch and B. Derby, *Adv. Mater.*, 2016, **28**, 7993-8000.
- 31 S. Zheng, X. Tang, Z.-S. Wu, Y.-Z. Tan, S. Wang, C. Sun, H.-M. Cheng and X. Bao, *ACS Nano*, 2017, **11**, 2171-2179.
- 32 S. Gao, K. Wang, Z. Du, Y. Wang, A. Yuan, W. Lu and L. Chen, *Carbon*, 2015, **92**, 254-261.
- 33 F. Miao, C. Shao, X. Li, K. Wang, N. Lu and Y. Liu, *J. Mater. Chem. A*, 2016, **4**, 5623-5631.
- 34 Y. Jiang, H. Shao, C. Li, T. Xu, Y. Zhao, G. Shi, L. Jiang and L. Qu, *Adv. Mater.*, 2016, **28**, 10287-10292.
- 35 X. Tang, H. Zhou, Z. Cai, D. Cheng, P. He, P. Xie, D. Zhang and T. Fan, *ACS Nano*, 2018, **12**, 3502-3511.
- 36 B. Xie, Y. Wang, W. Lai, W. Lin, Z. Lin, Z. Zhang, P. Zou, Y. Xu, S. Zhou and C. Yang, *Nano Energy*, 2016, **26**, 276-285.
- 37 Y. Jiang, Z. Xu, T. Huang, Y. Liu, F. Guo, J. Xi, W. Gao and C. Gao, *Adv. Funct. Mater.*, 2018, **28**, 1707024.